Supplementary Information

Underlayer engineering into the Sn-doped hematite photoanode for facilitating carrier extraction

Zhongyuan Zhou,[a,b] Shaolong Wu,[a,b,*] Chenhong Xiao,[a,b] Liujing Li,[a,b] and Xiaofeng Li[a,b,*]

[a]*School of Optoelectronic Science and Engineering & Collaborative Innovation Center of Suzhou Nano Science and Technology, Soochow University, Suzhou 215006, China*

[b]*Key Lab of Advanced Optical Manufacturing Technologies of Jiangsu Province & Key Lab of Modern Optical Technologies of Education Ministry of China, Soochow University, Suzhou 215006, China*

[*]E-mail: shaolong_wu@suda.edu.cn; xfli@suda.edu.cn

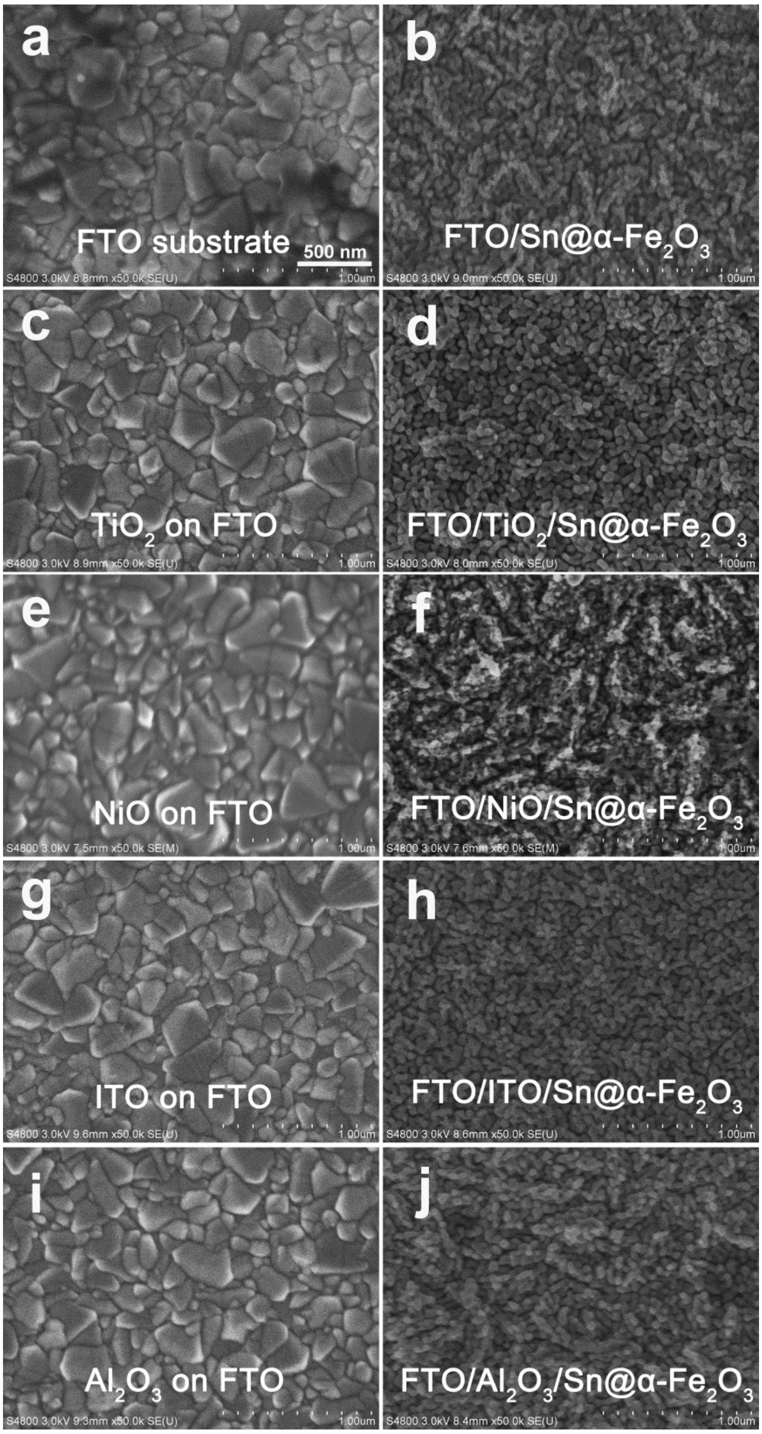

Fig. S1. Typical SEM images of various underlayers [(c) TiO_2, (e) NiO, (g) ITO and (i) Al_2O_3] deposited on (a) FTO substrate, and the corresponding SEM images of the post-grown Sn doped hematite film [(b) FTO/Sn@α-Fe_2O_3, (d) FTO/TiO_2/Sn@α-Fe_2O_3, (f) FTO/NiO/Sn@α-Fe_2O_3, (h) FTO/ITO/Sn@α-Fe_2O_3 and (j) FTO/Al_2O_3/Sn@α-Fe_2O_3].

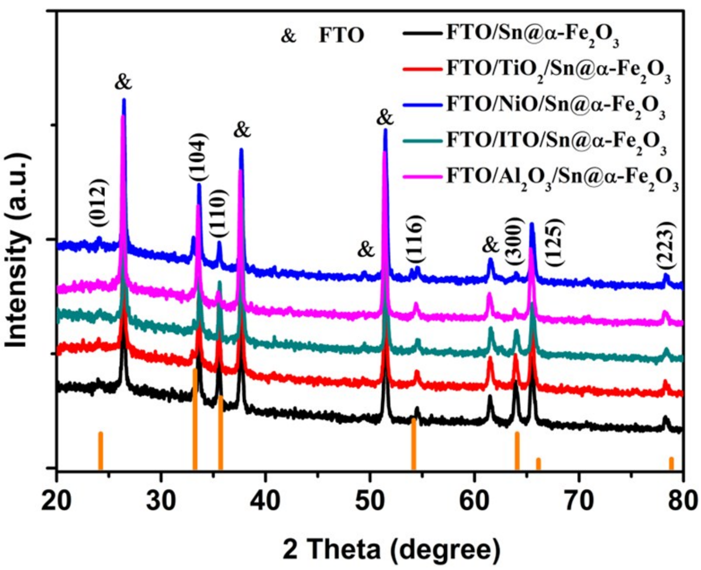

Fig. S2. XRD patterns of FTO/Sn@α-Fe_2O_3, FTO/TiO_2/Sn@α-Fe_2O_3, FTO/NiO/Sn@α-Fe_2O_3, FTO/ITO/Sn@α-Fe_2O_3 and FTO/Al_2O_3/Sn@α-Fe_2O_3 photoanodes.

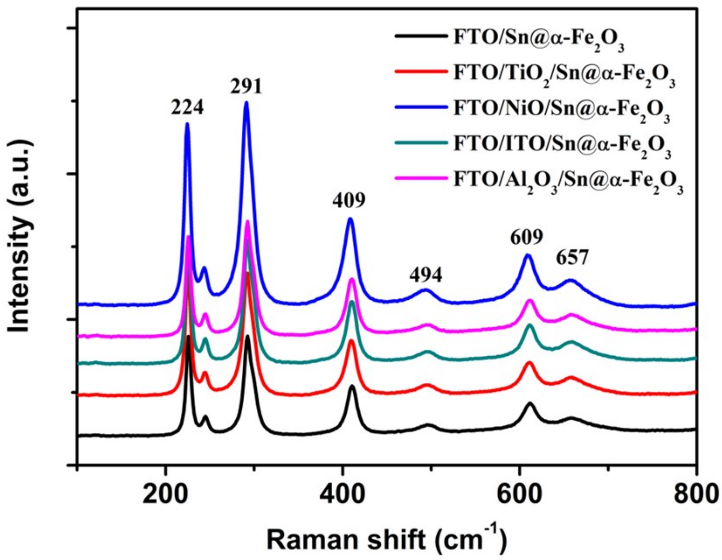

Fig. S3. Raman spectra of FTO/Sn@α-Fe_2O_3, FTO/TiO_2/Sn@α-Fe_2O_3, FTO/NiO/Sn@α-Fe_2O_3, FTO/ITO/Sn@α-Fe_2O_3 and FTO/Al_2O_3/Sn@α-Fe_2O_3 photoanodes.

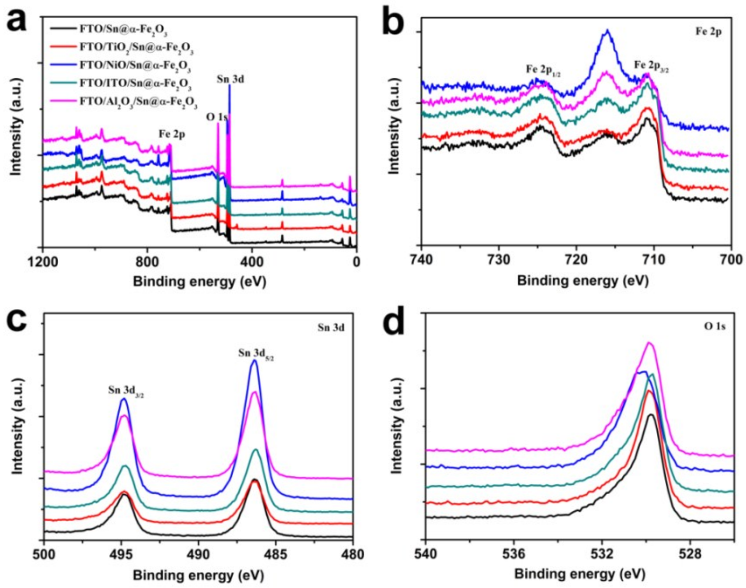

Fig. S4. (a) XPS spectra of FTO/Sn@α-Fe_2O_3, FTO/TiO_2/Sn@α-Fe_2O_3, FTO/NiO/Sn@α-Fe_2O_3, FTO/ITO/Sn@α-Fe_2O_3 and FTO/Al_2O_3/Sn@α-Fe_2O_3 photoanodes. (b–d) are the Fe 2p, Sn 3d and O 1s spectra in varying-underlayer photoanodes, respectively. Note that both of the positions and intensities of the Fe 2p, Sn 3d and O 1s peaks for various samples show slight changes due to the element doping from the underlayer.

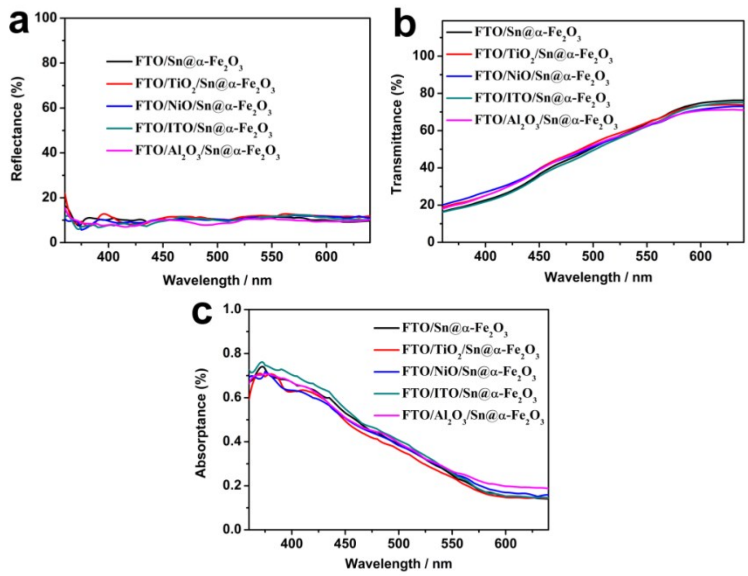

Fig. S5. (a) Reflectance, (b) transmittance and (c) absorption spectra of FTO/Sn@α-Fe_2O_3, FTO/TiO_2/Sn@α-Fe_2O_3, FTO/NiO/Sn@α-Fe_2O_3, FTO/ITO/Sn@α-Fe_2O_3 and FTO/Al_2O_3/Sn@α-Fe_2O_3 photoanodes. Absorption is calculated by unit subtracting the sum of reflectance and transmittance.

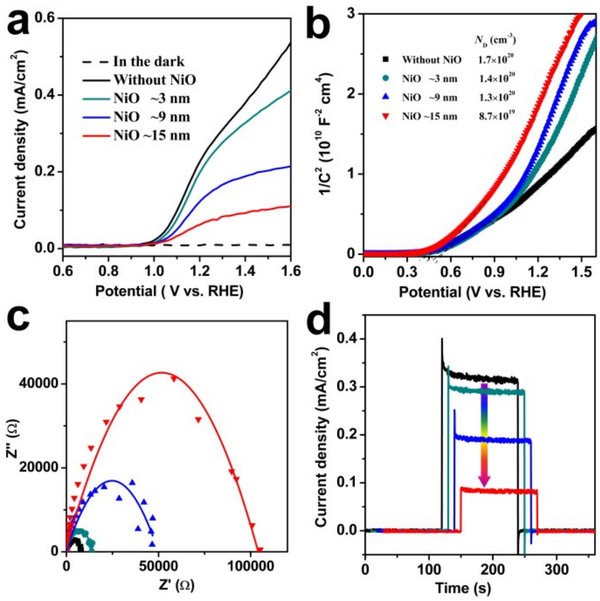

Fig. S6. (a) *J-E* curves, (b) Mott-Schottky curves, (c) PEIS plots at 1.23 V_{RHE}, (d) transient current density at 1.5 V_{RHE} between light-ON and light-OFF states for the FTO/NiO/Sn@α-Fe_2O_3 photoanodes with different thicknesses of NiO underlayer.

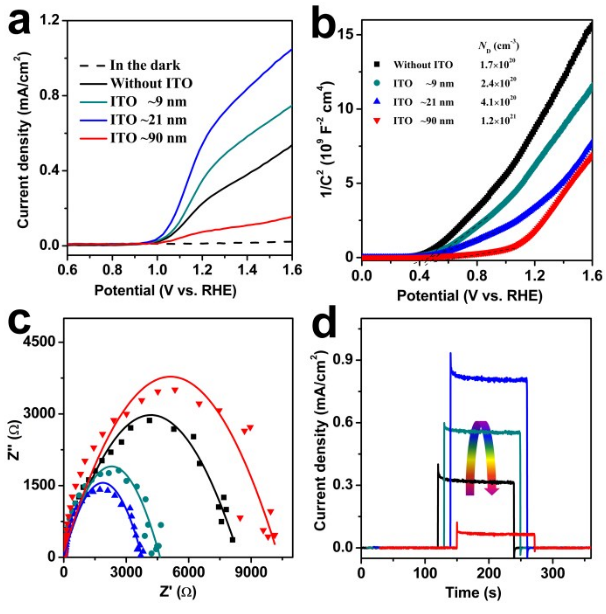

Fig. S7. (a) *J-E* curves, (b) Mott-Schottky curves, (c) PEIS plots at 1.23 V_{RHE}, (d) transient current density at 1.5 V_{RHE} between light-ON and light-OFF states for the FTO/ITO/Sn@α-Fe_2O_3 photoanode with different thicknesses of ITO underlayer.

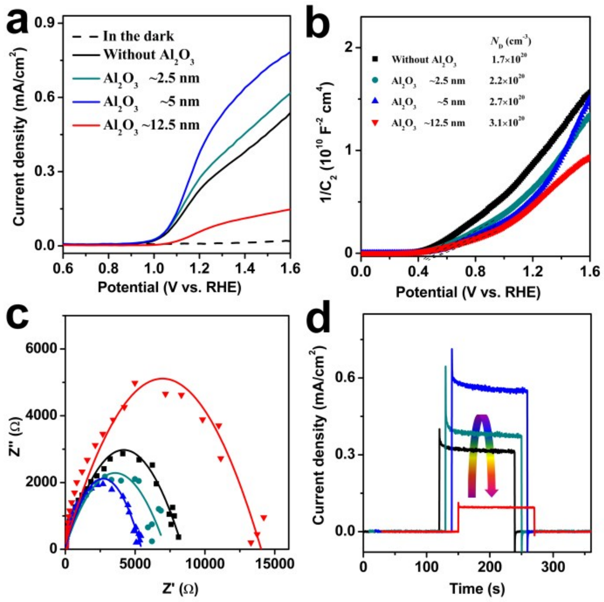

Fig. S8. (a) *J-E* curves, (b) Mott-Schottky curves, (c) PEIS plots at 1.23 V_{RHE}, (d) transient current density at 1.5 V_{RHE} between light-ON and light-OFF states for the FTO/Al_2O_3/Sn@α-Fe_2O_3 photoanode with different thicknesses of Al_2O_3 underlayer.

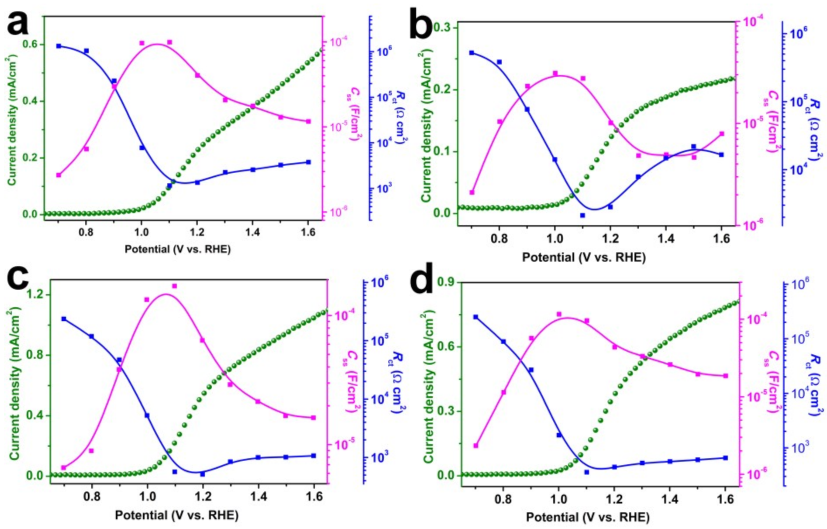

Fig. S9. Onset potential is consistent with the C_{ss} peak and the R_{ct} valley for the (a) FTO/Sn@α-Fe_2O_3, (b) FTO/NiO/Sn@α-Fe_2O_3, (c) FTO/ITO/Sn@α-Fe_2O_3 and (d) FTO/Al_2O_3/Sn@α-Fe_2O_3 photoanodes.

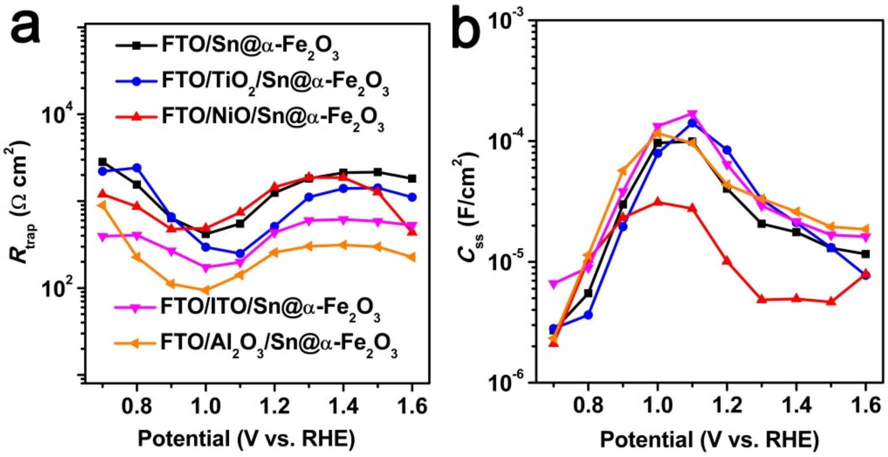

Fig. S10. Fitting values of (a) R_{trap} and (b) C_{ss} based on the equivalent circuit model.

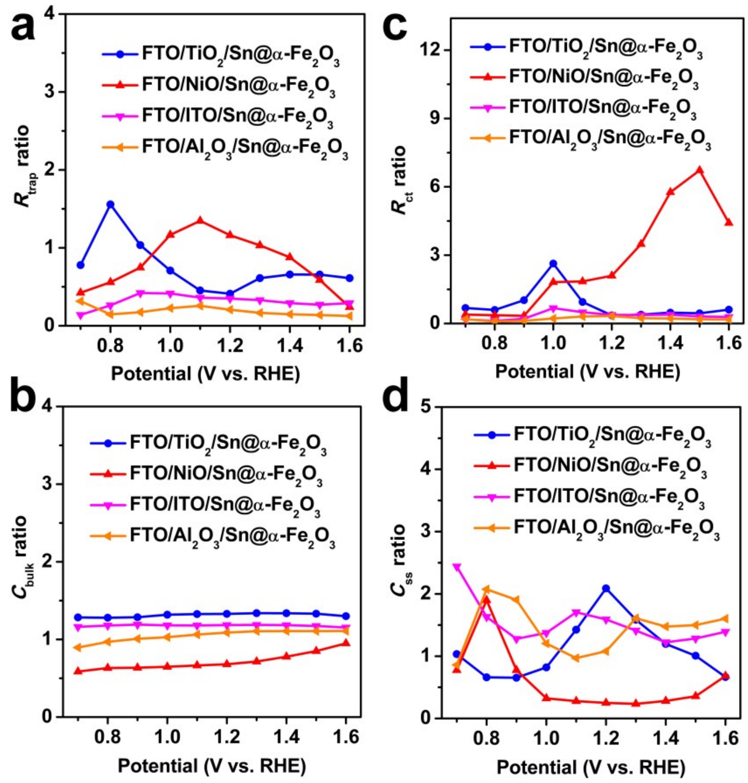

Fig. S11. The ratios of (a) R_{trap}, (b) C_{bulk}, (c) R_{ct} and (d) C_{ss} for the varying-underlayer photoanodes relative to the FTO/Sn@α-Fe_2O_3 photoanode.

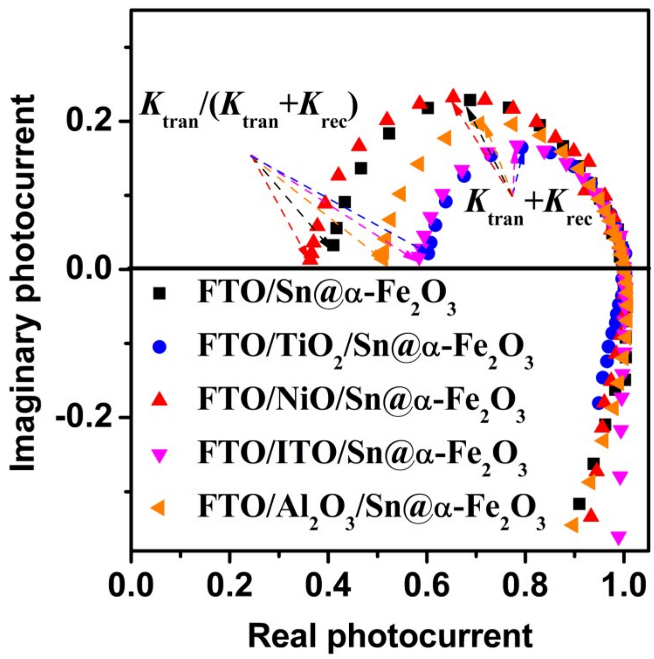

Fig. S12. IMPS plot at 1.23 V_{RHE} for FTO/Sn@α-Fe_2O_3, FTO/TiO_2/Sn@α-Fe_2O_3, FTO/NiO/Sn@α-Fe_2O_3, FTO/ITO/Sn@α-Fe_2O_3 and FTO/Al_2O_3/Sn@α-Fe_2O_3 photoanodes under the illumination of an UV LED.

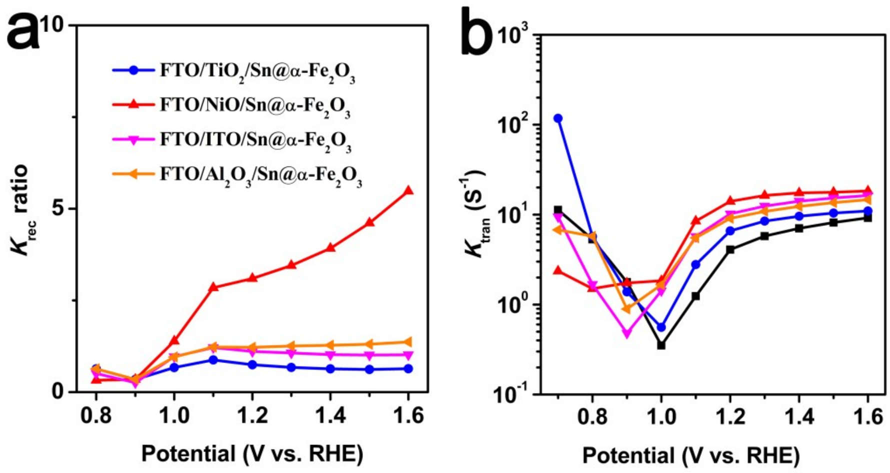

Fig. S13. (a) A ratio of K_{rec} for the varying-underlayer photoanodes relative to the FTO/Sn@α-Fe_2O_3 photoanode. (b) The transfer rate constant (K_{tran}) based on the IMPS plots.